3D-Printed External Light Trap for Solar Cells Supplementary Information

Lourens van Dijk[1], Ulrich W. Paetzold[2], Gerhard A. Blab[3], Ruud E.I. Schropp[4] and Marcel Di Vece[1]

[1]Nanophotonics - Physics of Devices, Debye Institute for Nanomaterials Science, Utrecht University, High Tech Campus, Building 21, 5656 AE Eindhoven, The Netherlands

[2]Institut für Energie- und Klimaforschung 5 – Photovoltaik, Forschungszentrum Jülich GmbH, 52425 Jülich, Germany

[3]Molecular Biophysics, Debye Institute for Nanomaterials Science, Utrecht University, Princetonplein 1, 3584 CC Utrecht, The Netherlands

[4]Eindhoven University of Technology (TU/e), Department of Applied Physics, Plasma and Materials Processing, 5600 MB Eindhoven, The Netherlands

I. Supplementary Information

A. Fabrication: 3D-Printing & Silver Coating

The CAD design of the external ligth trap was made using OpenSCAD [1]. Cura, a so-called *slicer*, converts the CAD file to ~10^5 print lines [2]. The extrusion speed of the molten plastic is also calculated by the slicer. A tabletop *Ultimaker Original* 3D-printed the CPCs and the cage [3]. The printer consists of a print head which moves in a horizontal plane constituting the x and y direction of the object. The plastic is printed on a platform that moves one step of around 50 to 200 μm downwards after finishing each layer. The width of the print line is determined by the nozzle ($\varnothing\sim400\,\mu$m). The print head heats the ABS to a temperature of around 260°C. The molten thermoplastic is extruded and deposited as a line on the printing platform. The track of the head depends on several settings like nozzle ø, layer height and filling fraction. The thermoplastic attaches to the platform and/or the already printed part and solidifies. A movie of the printing process can be found in another supplementary file. To obtain a proper bonding of the plastic, we applied *Scotch 3M Blue Tape 2090* to the platform. The print was cut loose from the platform and cleaned with ethanol to remove any residual tape. The light trap was metalized with 400 nm of silver using an EMITECH K575X sputter coater.

Chemical Smoothening. For the smoothening of the Acrylonitrile Butadiene Styrene (ABS), acetone was put into a jar standing on a heated stove above the boiling point of acetone ($T\sim90\,^\circ$C). After several minutes, acetone condensate emerges at the (relatively cool) glass jar. Then, the 3D-printed light trap is inserted into the jar for several minutes and exposed to the acetone vapor. This process is repeated several times. The initial temperature of the printed object is critical, as the warm and saturated vapor condenses quickly on cool surfaces. An ice pack was used to reduce the ABS temperature before inserting the model into the jar. The main smoothening occurs in the first seconds due to heavy condensation of the acetone. The acetone dissolves the ABS surface. The liquidized ABS on the surface lowers its surface energy by forming a smooth surface.

B. Design Parameters of the Light Trap

Shifted Compound Parabolic Concentrator. The concentration factor is enhanced further by shifting the paraboloid sides radially inwards by Δr, as shown in Fig. 3a. The focal point is shifted Δr outward in the radial direction and a non-imaging focal ring emerges. A shift of $\Delta r = r_{\text{aperture}}/2$ relocates the focal point of each CPC side exactly below the edge of the opposite side. Accordingly, A_{aperture} $\left(=\pi\cdot\frac{r^2_{\text{aperture}}}{2^2}\right)$ is reduced by a factor $\chi_{\text{shift}}=4$. Thereby, the concentration factor is multiplied by χ_{shift} (eq. 2). To prevent severe optical loss by inaccuracies in the printed design we set χ_{shift} to 3. Combining this χ with a 2× parabolic shape yields a trapping factor $C=2\cdot3=6\times$. The corresponding angle of incidence at the cell ranges from 20° to 37°.

Shifted Parabolic Concentrator & Acceptance Angle. We note that Eq. 5 cannot be directly applied to the shifted CPC, because a shifted CPC does not have a well-defined $\theta_{\text{acceptance}}$: for a certain range of angles of incidence the light is only partly transmitted to the solar cell. However, it is a useful estimation and the inversely proportional relation between the acceptance chance and the maximum path length enhancement, holds in general.

Choice of Concentration Factor of the CPC. Fabrication defects of the CPC translate to escape losses in the CPC, as the light does not follow the intended optical path. This production related problem becomes more pronounced when the distance between the point at which the light reflects at the CPC and the aperture increases. Conventional CPCs become rather tall for high concentration factors [4] and thereby the achievable transmission is thus reduced. To prevent this escape loss, the shape of the concentrator was adapted by shifting

both parabola sides inwards. Due to the relative short height of this concentrator, this permits a relative high transmittance, even at a high concentration factor. The optimization of the concentration factor of the light trap is thus primarily a trade-off between the negative effects of design inaccuracies on the CPC transmission and the improved absorption due to path length enhancement.

Cage. The inner dimensions of the square cage are 9×9 mm^2 to enable proper alignment on top of the 10×10 mm^2 solar cell. For the measurements of the bare solar cell the cage is used as a mask with an area of 9×9 mm^2 which defines an equal optically active solar cell area. The circular opening area of the concentrator (A_{CPC}) and the (horizontal) inner area of the square cage (A_{cage}) are both 81 mm^2. The CPC radius (in mm units) is therefore set to:

$$r_{\mathrm{cpc}}=\sqrt{\frac{A_{\mathrm{cage}}}{\pi}}\left(=\sqrt{\frac{81\,\mathrm{mm}^2}{\pi}}\right).$$

The area and the corresponding incident photon flux is thus equal for the bare cell (with the cage used as a mask) and the light trap on top (the cage and the CPC). Thereby there is only a contribution due to the light trapping. There is no concentration effect because the square area of the masked cell equals the circular opening area of the CPC.

Cage Height. Suppose an imaginary case in which the focal point of a paraboloid is located at the solar cell. In that case the incident light reflected by the cell propagates to the opposite side of the CPC and escapes without being trapped. To prevent this direct escape, a certain cage height (h_c) is needed between the aperture of the CPC and the solar cell. This condition is relaxed in the case of a shifted compound parabolic concentrator, as there the focal ring is shifted radially outwards with respect to the central axis which prevents a direct escape of the light. The cage height is set to 5 mm which enables the beam to expand to an area larger than $A_{aperture}$ at the solar cell. In this way, the reflected light will hit the reflective cage wall, instead of escaping through the aperture. To prevent this direct escape the cage height has to be sufficiently larger than the focal height.

CPC Design Parameters. Here, we discuss several design considerations of the light trap. The formula for the height (z) of a concentrating parabola is:

$$z(r)=\frac{1}{4f}r^2, \tag{6}$$

with r the radius and f the focal distance measured from $z=r=0$. For a 3D-paraboloid with a top radius (r_{top}) and a concentration factor (C) (see eq. 2), the aperture radius (r_{a}) is given by $r_{\mathrm{a}}=\frac{r_{\mathrm{top}}}{\sqrt{C}}$. To obtain a desired degree of trapping, the paraboloid is truncated at a height z_{tr}, with $z_{\mathrm{tr}}>f$. In case $z_{\mathrm{tr}}=f$ the paraboloid will make a 45° angle with the horizontal at the truncated paraboloid bottom side (see bottom of Fig. 3a) and the light is thus reflected horizontally. The large angle of incidence at the cell results in higher reflection on the cell interfaces according to the Fresnel equations (see Fig. 5). This problem is also known in image sensors as pixel vignetting. This problem can be solved by truncating the paraboloid higher, at $z_{\mathrm{tr}}=f+\Delta z$. We set Δz such that the range of *AOI* shifts towards the normal at which the cell has a relative low reflectance. To find a proper f and z_{tr} the following equation is solved for f:

$$(z_{\mathrm{tr}}=)\frac{1}{4f}\left(\frac{r_{\mathrm{top}}}{\sqrt{C}}\right)^2=f+\Delta z$$
$$\therefore f=\frac{\sqrt{C^2\cdot\Delta z^2+C\cdot r_{\mathrm{top}}^2}-C\cdot\Delta z}{2\cdot C}$$

C. Irradiance Distribution and External Light Trapping.

Due to the use of the concentrator the illumination distribution at the solar cell can become inhomogeneous. Therefore, the current generation in the cell is also inhomogeneous. This results in inhomogeneous current generation in the cell, leading to an elevated impact of the series resistance. This potential problem can be reduced by using an optimized trap design. When a tall cage is used the light diverges significantly, and it will therefore illuminate a larger cell area when it reaches the solar cell for the first time. Another solution that enables uniform and near normal illumination has been described earlier [5]. Here, two CPCs are directly connected at their short aperture. The upper CPC focuses the light and the bottom one forms a cage that redistributes the light evenly. This design can be beneficial due to the more normal incidence at the cell level. A disadvantage is that the light generally is reflected more often at the cage compared to other designs [6, 7].

D. Error Propagation in the Focal Point due to Deformations of the Concentrator

During the production of the CPC, several deformations can arise compared to the intended design. For example, a temperature change can deform the CPC. For the proper functioning of the CPC it is important to examine the effect of deformations from the intended shape, eq. 6, on the optical properties.

A linear deformation of the parabolic concentrator in the z-direction results in $z_{\mathrm{deformed}}=z\cdot\circledast$. The focus shifts accordingly:

$$z_{\mathrm{deformed}}=\frac{1}{4f}r^2\cdot\circledast$$
$$\therefore z_{\mathrm{deformed}}=\frac{1}{4(f/\circledast)}r^2$$

It becomes clear that for a deformation $\circledast > 1$ the shape corresponds to a parabola with a *downward* shifted focal point ($f/\circledast$=constant).

A linear deformation in the *radial* direction results in:

$$z_{\text{radially deformed}} = \frac{1}{4f}(r/\circledast)^2$$
$$\therefore z_{\text{radially deformed}} = \frac{1}{4(f\cdot\circledast^2)}r^2$$

Here, a positive radial stretch with a radial deformation $\circledast > 1$ corresponds to a parabola with an *upwards* shifted focal point.

E. Cell Design: Considerations & Fabrication

The functionality of the trap is tested on a 1.2 μm thick superstrate (p-i-n) nc-Si:H solar cell. The 10×10 mm^2 cell can be electrically contacted from the back side, such that it does not conflict with the placement of the light trap as we explain here.

For solar cells made in a substrate configuration, the placement of the electrical probes at the sun-facing side can interfere with the placement of the light trap. This experimental complication for substrate cells can be circumvented by making electrical contact pads besides the solar cell and light trap. To circumvent this complication of substrate cells, we decided to fabricate a cell in superstrate configuration (see Fig. 5). This cell can be electrically contacted from the back side, such that the placement of the probes does not conflict with the placement of the external light trap.

For cells that do have reflective front contacts the shadow loss is reduced as a consequence of the optical recycling of the light trap. Thereby, an additional energy conversion efficiency enhancement (typically around 5 to 10%) can be expected. As we used a superstrate cell configuration, without metal fingers on top of the cell, we did not demonstrate this reduction of the shadow loss.

The cell is deposited on a Corning-Glas (Corning Eagle 2000) superstrate. A 700 nm thick ZnO:1%Al layer is sputtered at $\sim$430 °C by a radio-frequency magnetron sputtering. The silicon material is deposited at a radiofrequency of 13.56 MHz using PECVD: *p*-layer ($\sim$20 nm); *i*-layer ($\sim$1200 nm); *n*-layer ($\sim$20 nm) [8–12]. The back contact consist of a 80 nm RF-sputtered ZnO:0.5%Al and 700 nm of thermally evaporated Ag. The cell area is defined by 10 mm $\times$ 10 mm deposited silver back contact. The light trap was placed on top of the unprocessed side of the glass while the cell was contacted from the backside of the glass.

F. Determination of the Path Length Enhancement Factor

Here, we describe the experimental determination of Π_{ext} using the implied absorptance derived from the *EQE* and *IQE*. The *EQE* of a cell with external light trap (EQE_{trap}) is defined as the total number of collected charge carriers, divided by the number of incoming photons (at the top of the CPC). The path length enhancement can be calculated from the bare cell absorptance (A_{bare}) and the total absorptance of the cell with the external light trap (A_{trap}). However, it is experimentally difficult to measure A_{trap} directly, as A_{trap} is optically indistinguishable from the parasitic absorptance by the CPC and the cage. However, A_{trap} can be estimated from the EQE_{trap} using the *IQE*:

$$A_{\text{trap}} = EQE_{\text{trap}}/IQE,$$

we assume that IQE_{bare} and IQE_{trap} are equal.

After determining the absorptance, the path length enhancement factor can be calculated. In first order, the absorptance is described by the Beer-Lambert law. For light that passes the solar cell Π_{ext} times, the net reflectance R_{trap} as observed outside the trap, is thus given by $(R_{\text{sc}})^{\Pi_{\text{ext}}}$. For an idealized light trap Π_{ext} can be estimated from the measured EQE_{trap} and A_{sc} according to:

$$R_{\text{trap}} = (R_{\text{sc}})^{\Pi_{\text{ext}}}$$
$$1-A_{\text{trap}} = (1-A_{\text{sc}})^{\Pi_{\text{ext}}} \quad (7)$$
$$1-\frac{EQE_{\text{trap}}}{IQE} = (1-A_{\text{sc}})^{\Pi_{\text{ext}}} \quad (8)$$
$$\therefore \Pi_{\text{ext}} = \frac{\log(1-\frac{EQE_{\text{trap}}}{IQE})}{\log(1-A_{\text{sc}})}. \quad (9)$$

Parasitic Losses. The *EQE* of the cell with external trap (EQE_{trap}) is related to the absorptance according to:

$$EQE_{\text{trap}} = IQE\cdot A_{\text{trap}} = (1-IPL)\cdot A_{\text{trap}}, \quad (10)$$

with *IPL* the internal (optical and electrical) parasitic losses. These parasitic losses are ascribed to both the absorption in the non-active layers and the non-collected (recombined) charge carriers. Notice that the *IQE* is indeed the upper limit for EQE_{trap} (when A_{trap}=1). A_{trap} converges to 1 at moderate ($5-10\times$) trapping factors, see Fig. 2.

The *IQE* is related to the carrier collection efficiency (f_{c}) and to the absorption in the active layer (A_{active}):

$$IQE = \frac{f_{\text{c}}\cdot A_{\text{active}}}{A_{\text{sc}}} = \frac{f_{\text{c}}\cdot A_{\text{active}}}{A_{\text{active}}+A_{\text{p}}},$$

with A_{p} the parasitic absorption in non-active layers. A high value of f_{c} and a low A_{p} are therefore essential for a high *IQE*. The parasitic absorptance in textured solar cells is generally higher than in flat cells.

Path Length Enhancement as Function of the Absorptance. The achievable path length enhancement factor depends on the cell reflectance. From eq. 3 and eq. 4 the expected theoretical maximum of Π_{ext} was calculated. Fig. 9 illustrates that the path length enhancement factor is inversely

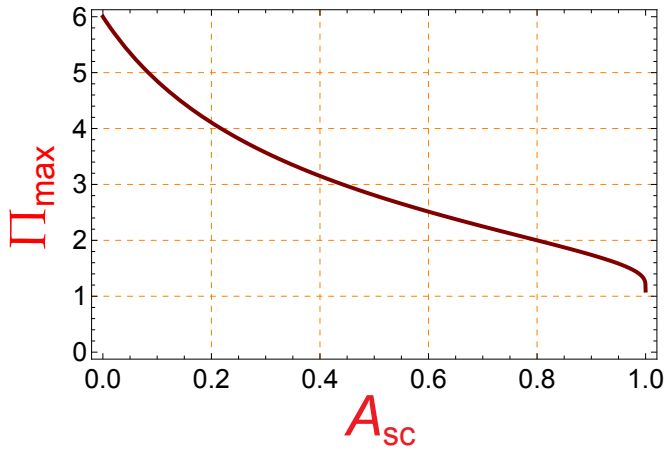

Figure 9: Plot of the simulated maximum achievable path length enhancement factor Π_{max} for a perfect concentrator and trap as a function of the absorptance of the bare solar cell (without a light trap).

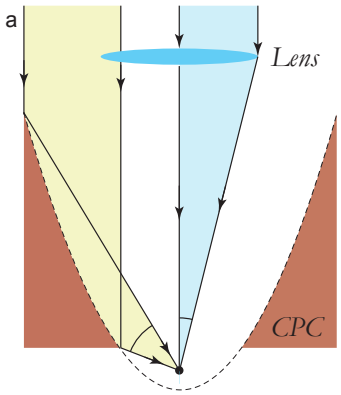

Figure 10: Illustration for comparison of a lens and a parabolic concentrator. The *NA* of the drawn lens is 0.25. In 3D the indicated area is a cone.

related to the absorptance.

G. Design Considerations for the 3D-Printed Compound Parabolic Concentrator and the Cage

There are several options for the concentrator of the light trap: (Fresnel-) lenses, (compound) parabolic concentrators etc. Microlens arrays, as used in CMOS imaging and wavefront sensors [13], are interesting options. However, they are not expected to be optimal due to their relative low transmittance, relative long focal length and low numerical aperture (*NA*).

There is a significant difference between metalized CPCs and dielectric lenses regarding the angular distribution of the light. A lens refracts the light to a centric cone with a relative small angle around the concentrator axis, indicated by the blue area in Fig. 10. In contrast, for CPCs light is coming from larger angles with respect to the concentrator axis, indicated by the yellow area. The relative long focal distance of refractive lenses makes it technically difficult to align the concentrator and the aperture. An advantage of metalized CPCs over dielectric concentrators is that both the concentrator and the aperture are formed (in one production process) into one single piece. No additional alignment of the aperture and concentrator is needed, as would be necessary for dielectric lenses. Due to the relative long focal distance (or low *NA)* of dielectric lenses, a relative tall cage would be needed to prevent light from escaping. Additionally, the angular cone is more tunable for CPCs as we exploited in this paper.

The reflection of the Ag coating of the CPC is high in the relevant part of the solar spectrum. At the same time, the geometric response is equal for all wavelengths; there is thus no chromatic aberration. Due to the optical characteristics of metals, one can reach high transmission efficiencies with hollow metalized paraboloids. Dielectric, solid CPCs with an anti-reflective coating can surpass the performance of metalized CPCs, as the parasitic absorption in the glass is low.

References

[1] OpenSCAD, CAD software; [cited 2014 Aug 8]. Available from: www.openscad.org.

[2] Cura, slicer software; [cited 2014 Aug 8]. Available from: http://software.ultimaker.com/.

[3] Ultimaker homepage; [cited 2014 Aug 8]. Available from: www.ultimaker.com.

[4] Winston R, Miñano JC, Benítez P. Nonimaging Optics. Electronics & Electrical. Elsevier Academic Press; 2005.

[5] Kosten ED, Atwater JH, Parsons J, Polman A, Atwater HA. Highly efficient GaAs solar cells by limiting light emission angle. Light Sci Appl. 2013;**2**:e45.

[6] Luque A, Miñano JC. Optical aspects in photovoltaic energy conversion. Sol Cells. 1991;**31**:237–258.

[7] Weinstein LA, Hsu WC, Yerci S, Boriskina SV, Chen G. Enhanced absorption of thin-film photovoltaic cells using an optical cavity. J Opt. 2015;**17**(5):055901.

[8] Rech B, Repmann T, Van den Donker M, Berginski M, Kilper T, Hüpkes J, et al. Challenges in microcrystalline silicon based solar cell technology. Thin solid films. 2006;**511**:548–555.

[9] Schropp R, Rath J, Li H. Growth mechanism of nanocrystalline silicon at the phase transition and its application in thin film solar cells. J Crystal Growth. 2009;**311**:760–764.

[10] Woerdenweber J, Merdzhanova T, Zimmermann T, Flikweert A, Stiebig H, Beyer W, et al. Cross-contamination in single-chamber processes for thin-film silicon solar cells. J Non-Cryst Solids. 2012;**358**:2183–2186.

[11] Moulin E, Paetzold UW, Kirchhoff J, Bauer A, Carius R. Study of detached back reflector designs for thin-film silicon solar cells. Phys Status Solidi-R. 2012;**6**:65–67.

[12] Zhang W, Paetzold UW, Meier M, Gordijn A, Hüpkes J, Merdzhanova T. Thin-film silicon solar cells on dry etched textured glass. Energy Procedia. 2014;**44**:151–159.

[13] Thorlabs homepage; [cited 2014 Aug 8]. Available from: www.thorlabs.com.